Sintering and grain growth in $SrTiO_3$: impact of defects on kinetics

Fabian Lemke, Wolfgang Rheinheimer and Michael J. Hoffmann

Abstract

In this study, the microstructural evolution of undoped and iron doped $SrTiO_3$ is analyzed during sintering at 1280°C in air and reducing atmosphere. The focus is on densification and grain growth during different holding times investigated by dilatometric sintering. The sintering equations developed by Coble are used to characterize sintering. The influence of defect chemistry on diffusion, densification and grain growth is evaluated using basic defect chemical equations. However, to understand sintering of perovskites a space charge concept at the grain boundaries needs to be added to the bulk defect chemistry, since the major part of mass transport during sintering occurs in this region. This extension of the defect chemistry allows for explaining the change in diffusion mechanism during sintering (grain boundary diffusion or bulk diffusion) as well as the grain growth stagnation observed in iron doped $SrTiO_3$.

These results are used to separate the complex interplay of densification and grain growth. While grain growth decreases with increasing defect concentration, for the densification kinetics no clear trend is observed, since both grain growth and diffusion are relevant. The results show that grain growth during sintering provides comparable results to grain growth experiments in dense $SrTiO_3$. The calculated diffusion coefficients are in good agreement with the literature and show a strong dependency on the concentration of strontium vacancies.

defect chemistry, sintering, microstructural evolution, grain growth, $SrTiO_3$, space charge, grain growth stagnation, diffusion

1   Introduction

Perovskite ceramics are widely used in different electronic applications like actuators (e.g. Lead zirconate titanate, $Pb[Zr_x,Ti_{1-x}]O_3$), sensors (doped Strontium titanate, $SrTiO_3$), and high-permittivity dielectrics (Barium titanate, $BaTiO_3$)[1, 2]. In the past decades $SrTiO_3$ has established as a model material for perovskite ceramics. Accordingly, basic properties as defect chemistry[3, 4, 5, 6], ionic conductivity[1, 3, 7, 8, 9, 10, 11], diffusion properties [12, 13, 14, 15, 16] and atomic structure of interfaces[17, 18, 19, 20, 21, 22, 23, 24] are well-known.

A full set of reaction constants for the high temperature bulk defect chemistry (1000°C-1400°C) in $SrTiO_3$ was measured by Moos and Haerdtl[6]. For the grain boundary in $SrTiO_3$, a model based on a positive, Ti-rich grain boundary core, leading to an adjacent space charge layer was proposed by Chiang and Takagi[17, 18] using results TEM results. Impedance data[25], SIMS measurements[10] and simulations[5] provide detailed data of the space charge properties. Values for the space charge width range from several nanometers up to 100 nm and the potential at the grain boundary is determined to values between 0.4 V and 1.0 V. A set of diffusion data for Ti and Sr in $SrTiO_3$ single crystals is presented by Goemann et al.[15, 16], which indicate the high temperature diffusion of both species via strontium vacancies. The only data for strontium vacancy motilies are presented by Poignant and Juda[26] for polycrystalline $(Sr,Ca)(Ti,Nb)O_3$ and Meyer et al.[27] in single crystal $SrTiO_3$.

In particular several studies of the microstructural evolution (i.e. densification and grain growth) are published for $SrTiO_3$ [28, 29, 30, 31, 32, 33, 34, 35]. The densification is mainly examined regarding the influence

of the Sr/Ti stoichiometry[28, 32]. For material with Sr excess grain growth seems to dominate the microstructural evolution even during densification, while in Ti-rich material densification is followed by grain growth. Both authors explained their findings with the influence of Sr excess and the formation of Sr vacancies leading to a decreasing diffusivity in the material. The appearance of a non-Arrhenius grain growth behaivior[29, 33] is another important fact for the development of the microstructure. A transition regime is found between 1350°C and 1425°C leading to bimodal grain growth. While the phenomena is not yet fully understood, the influence of the grain boundary energy[34], the mobility[35] and the grain boundary structure[30] are examined to find a proper explanation.

During processing, usually implicating a sintering procedure, the main characteristics of the materials such as microstructure and allocation of defects are defined. As these microscopic properties influence the macroscopic performance of the material, knowledge about the evolution of the material during processing is of great importance. Changes in the electrical conductivity from isolating up to conducting by addition of dopants and variations of the resistance of the material due to the influence of grain boundaries are only fragments showing that designing the sintering process and hence the microstructure, is a crucial point to achieve the required material properties.

An analytical model to characterize the microstructural development was given by Coble[36, 37, 38] linking the densification with grain size and diffusion constant. The changes in the microstructural evolution can be interpreted in two ways following the simplified coble equation

$$\dot{\rho} = C \cdot D/G^m \qquad\qquad (1)$$

with C being a constant, G the mean grain diameter and D the diffusion coefficient. The exponent m depends on the dominating diffusion mechanism and reaches $m = 3$ for volume diffusion and $m = 4$ for boundary diffusion[36, 37].

The variation in the densification behavior can be attributed to the diffusion coefficient D and diffusion mechanism or is caused by the change of the driving force like the curvature, free surface or interfacial energies. The diffusion coefficient might be changed by the changing sintering conditions and their influence on the defect chemistry while the free surface depends on the interaction of grain growth and densification for the studied material. While these effects will be treated separately in the following, they are most likely strongly dependent on each other during the microstructural evolution.

For the first time we make use of this model to analyze the intermediate stage of the sintering process of SrTiO₃. To separate densification and grain growth, we use iron doping to suppress grain growth. Comparing the sintering process at different doping levels and in reducing atmosphere offers the possibility to evaluate the influence of the defect chemistry on densification and grain growth. For grain growth some investigations exist on SrTiO₃ explaining changes in the microstructure with the total defect concentration by Chung et al.[39, 40]. While the work of Chung et al. focuses on oxygen vacancies, we propose strontium vacancies as dominant defect species for the diffusion leading to densification and grain growth following the findings of Goemann et al.[15, 16]. We also consider the existence of an internal space charge layer[17, 18, 23, 41] at the grain boundaries to explain some of our findings.

2 Experimental Procedure

Ceramic powders were prepared by the mixed oxide/carbonate route using $SrCO_3$ and TiO_2 as raw materials (purities of 99.95 and 99.995%, respectively; Sigma Aldrich Chemie GmbH, Taufkirchen, Germany). As acceptor dopant Fe_2O_3 (purity >99%, Merck, Darmstadt, Germany) was used. For undoped material the molar ratio of Sr/Ti was 0.996; for the doped samples the Sr/Ti ratio was 1.00 with Fe dopant concentrations of 2 at-% and 5 at-% with respect to the B site. The mixtures were milled with zirconia milling balls of 2 mm diameter and 2-propanol in an attrition mill. Calcining was done at 975°C for 6h in air. The results of the process were confirmed by XRD measurements, showing crystalline $SrTiO_3$ with no detectable second phase for all compositions. Particle sizes smaller around 500 nm in diameter result from 16 h milling with 10 mm diameter zirconia milling balls and 2-propanol in a planetary mill. The particle size was measured by laser diffraction (Cilas, 1064). SEM imaging provided information on morphology and agglomeration of powders.

Cylindrical green bodies for the dilatometer experiments were uniaxially pressed in a steel die and subsequently cold-isostatically pressed at 400 MPa. Green bodies showed densities between 61,2% and 63,8% calculated from geometry. Samples were approximately 12 mm long and 8 mm in diameter. Additionally, the green densities have been calculated backwards from the shrinkage data and the final density measured by the Archimedes method after sintering.

Sintering experiments were conducted in a single rod dilatometer (Netzsch, 402 E/2) in air (constant flow of 15 l/h) with a constant heating rate of 60 K to 1280°C followed by various dwell times (5 - 240 min). To compensate the thermal expansion of the alumina rod, a sapphire standard with 10 mm length was measured for each sintering setup. All sintering experiments were corrected with this data.

The density was determined by the Archimedes method after sintering. Every sintered sample was prepared for SEM imaging to observe microstructural appearance. Samples were cut and polished with different diamond grinding discs (30 µm – 2 µm) and cloths (1 µm and 0.25 µm, polycrystalline diamond slurry). Polished samples were thermally etched at 1075 °C for 2 h. The average grain size was measured at 500 or more grains per sample (AnalySis, Olympus, Japan).

## 3 Results and Discussion

3.1 Powder Characteristics

The particle size distributions and the corresponding SEM images of the powders are shown in Fig. 1. The median grain size as measured by d_{50} is between 0.40 µm and 0.60 µm and is smaller for the iron doped material. The SEM images indicate small differences in the particle morphology: while the undoped particles are more globular, the iron doped powders show a slightly plate-like geometry. The primary particle size as estimated from SEM images is 0.2 µm and therefor smaller than obtained by laser diffraction, which is most likely caused by a slight agglomeration of particles.
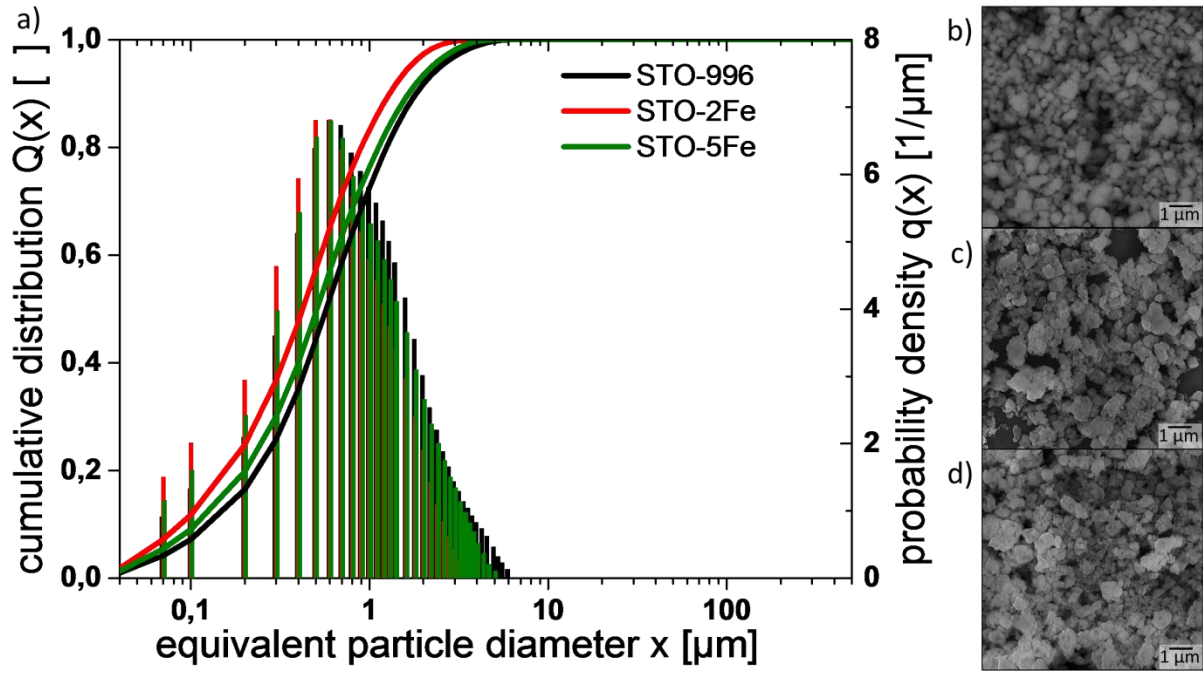
Fig. 1: Particle size distribution (a) and SEM images of the undoped (b), 2%-iron doped (c) and 5%-iron doped (d) SrTiO₃ powder.

3.2 Densification and Microstructural Evolution

In Fig. 2, densification and temperature curves for 120 minutes are compared for the different materials and sintering atmospheres. For the same temperature profile, the powder with 2% iron shows higher densification compared to the undoped material, while 5% iron leads to a drastic decrease in absolute density. In reducing atmosphere, the densification of undoped SrTiO₃ is lower than in oxidizing atmosphere. The isothermal densification rate reveals the difference in the densification characteristics best (Fig. 2 b). All compositions have comparable initial densification rates which decrease with time. This general decrease is caused by the reduction of free surface during sintering and, thus, a decrease of the driving force. In reducing atmosphere, the undoped SrTiO₃ shows slightly higher densification rates compared to sintering in air. With higher acceptor dopant concentration sintering rates decrease.
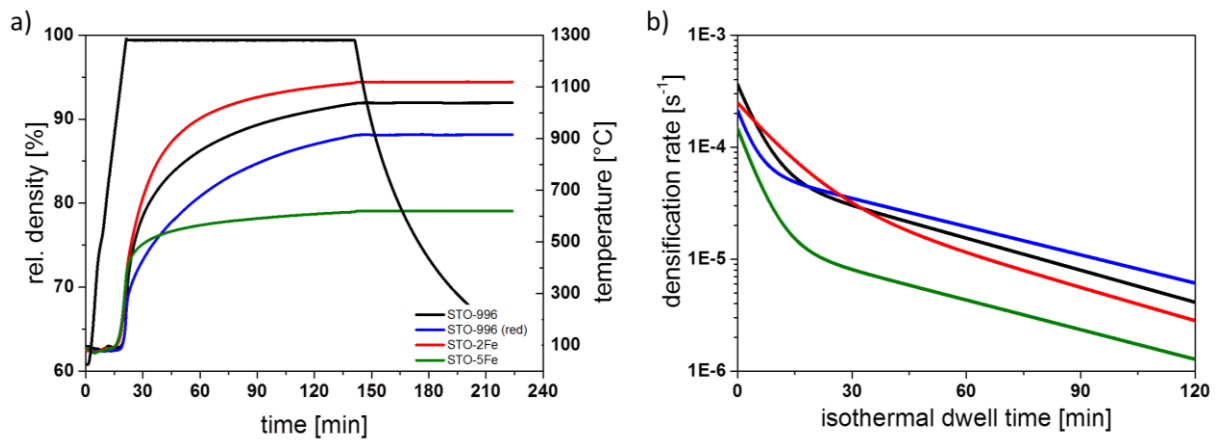

Fig. 2: Temperature and relative density for the 120 min isothermal cycle of all materials and sintering atmospheres (a). Derived densifications rates during the isothermal dwell time (b).

However, Fig. 2 a only shows densification over time, but ignores a change of the driving force for sintering caused by grain growth and densification. Therefore, the densification rate was determined for different dwell times during isothermal sintering and is shown in Fig. 3 with respect to grain size (a) and density (b).

The graph shown in Fig. 3 a allows for discriminating the dominant diffusion mechanism by observing the slope of the fitted lines: Volume diffusion results in a slope of $m = 3$ and grain boundary diffusion in $m = 4$.[37] Accordingly, for doped and undoped samples sintered in air, boundary diffusion seems to be dominant, while undoped material in reducing atmosphere shows a lower slope indicating a volume diffusion mechanism. At a representative grain size of approximately. 0.3 µm, the densification rate of undoped $SrTiO_3$ is highest, while iron doped materials shows significantly lower densification rates, which is in good agreement to the trend in Fig. 2. Since densification rates are very different at the same mean grain size (i.e. for similar driving forces), the diffusion coefficients must be different as well.

For a dopant concentration of 5%, grain growth is inhibited completely; accordingly the sintering equations by Coble[37] do not allow for a determination of the dominant diffusion mechanism. The effect of growth stagnation is known for undoped material as well, but at much larger grain sizes ###cite: Nr. 32### and will be addressed later.

The decrease in free surface area and therefor the sintering rate cannot only be attributed to grain growth, but also to the increase in density (i.e. a change in free surface area). Accordingly, Fig. 3 b) shows the densification rate with respect to relative density. All curves (but not for 5% Fe dopant) are very similar indicating a similar dependence of the densification rate from the free surface area. However, the decrease in densification rates of 5% Fe-doped $SrTiO_3$ is only related to the relative density. In contrast to Fig. 3a or Fig. 2 b, the 2% Fe-doped material now shows the highest densification rates.
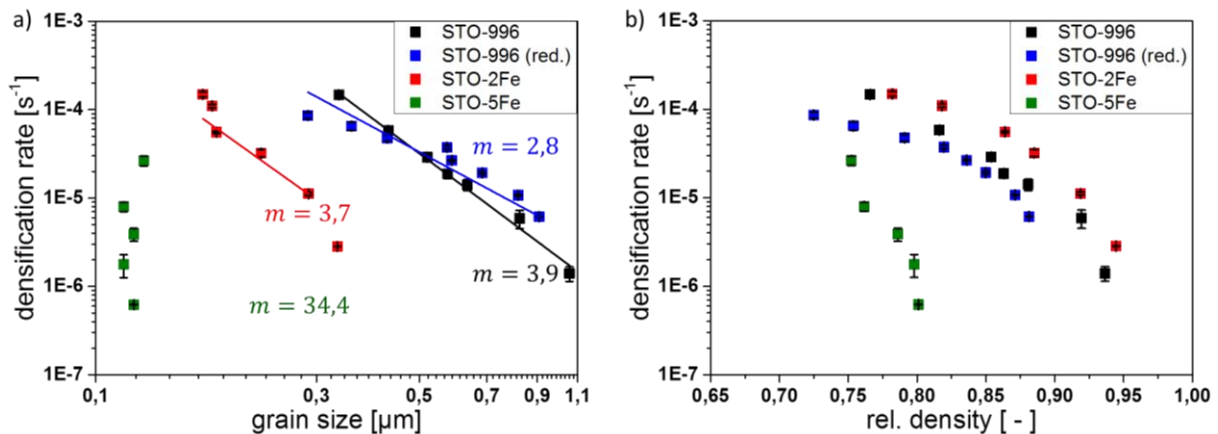

Fig. 3 Plot of the measured densification rate versus grain size (a) and relative density (b) for different dwell times.

To capture microstructural appearance, Fig. 4 shows SEM images of short and long dwell times. For undoped material (Fig. 4a-d), no significant change with atmosphere or dwell time can be observed other than an increase in density or grain size (cf. Fig. 2 and 9). With increased iron dopant concentration, a drastic change in the microstructure evolution occurs: For 2% Fe dopant (Fig. 4e and f), a much finer pore and grain size distribution is observed in the initial state of sintering. For long dwell times (Fig. 4f), still a small but bimodal grain size distribution is found with very small pores located at triple junctions. Grain growth occurred in areas, where few pores remained; accordingly small grains can be found in prorous regions. For 5% Fe-dopant, no significant grain growth occurs;

the mean grain size is the same in Fig. 4g and h. However, the morphology in Fig. 4g and h is very different from Fig. 4a-f: Densification occurs in clusters, which are sintered to allmost full density. In between, pores much larger than the average grain size exist. . Note that, ignoring the pore size, the mean grain size would imply fast shrinkage, which does not occur according to Fig. 2. This is discussed in Section 3.4.
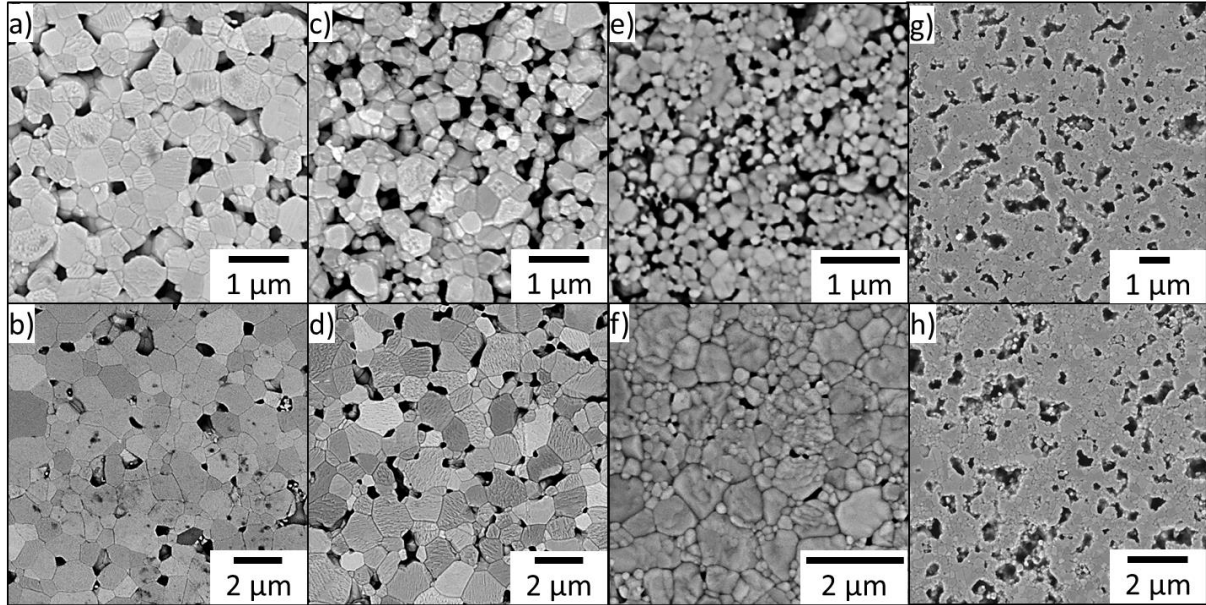
Fig. 4: Microstructures (5-240 min)

Fig. 5 gives the relationship between grain growth and density. Although grain growth is slightly faster in reducing atmosphere, no strong impact of the atmosphere was found and grain growth occurs simultaneously with sintering. For 2% Fe-doped $SrTiO_3$, no significant grain growth is visible below 80-85% relative density. Subsequently, as shown in Fig. 4e and f, single grains start to grow leading to an increase in the mean grain size accompanied by further densification. No grain growth occurs for 5% Fe-doped $SrTiO_3$.
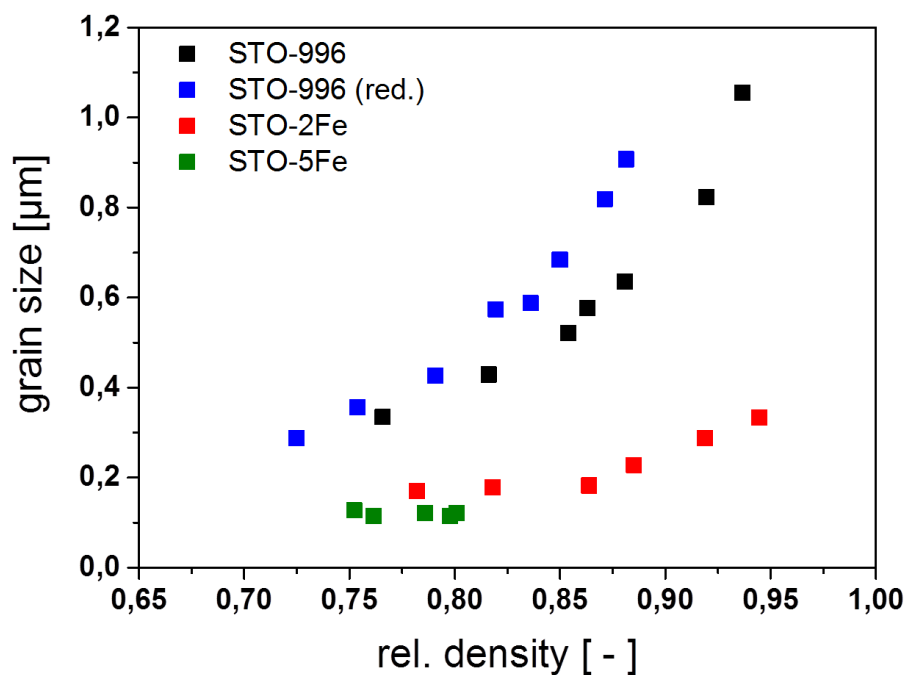
Fig. 5 grain size vs. density

3.3 Diffusion and Defect Chemistry in Sintering

In general, the Coble model allows for evaluating diffusion coefficients. The values are calculated with equation (1) for bulk diffusion using the measured grain size and densification rates from Fig. 3 a). Following the suggestion by Coble[36] the constant C in equation (2) can be written as

$$C = \left[\frac{720\gamma\Omega}{k_B T}\right]. \tag{2}$$

The interfacial energy γ is assumed with $1\ J/m^2$ and the atomic volume Ω corresponds to the volume of a perovskite unit cell $(a_0^3)_{\mathrm{SrTiO_3}} = 5{,}94 \cdot 10^{-29}\ m^3$. Since estimating a reasonable grain boundary width relevant for sintering is not possible and this parameter is a scale factor in the Coble equation for boundary diffusion, all calculations assume bulk diffusion to dominate during sintering.

The diffusion coefficients obtained from Fig. 3a are shown in Fig. 6. For undoped material the diffusion coefficient is independent of grain size, while with increasing dopant concentration lower diffusion coefficients are calculated with increasing grain size.
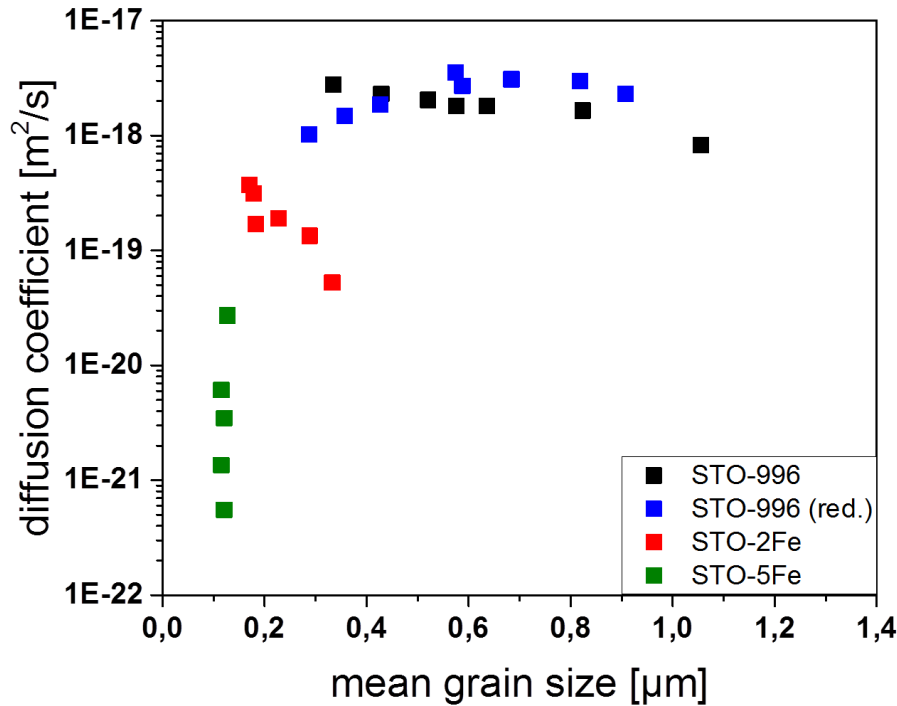
Fig. 6: diffusion coeficient vs grian size

In the literature, the lattice diffusion constant of Sr in SrTiO$_3$ was measured by tracer methods and was found to be in the order of $10^{-23} - 10^{-20}\ m^2/s$ at 1280°C[15, 16]. In the present sintering experiments the diffusion coefficients at the same temperature are higher by two orders of magnitude. Higher diffusion coefficients in sintering experiments compared to tracer data are a well known[38, 42, 43]; this is probably attributed to the influence of the microstructure and the difference in the driving force between the experimental setups. The Coble equation bases on many assumptions and should therefor only be seen as an order of magnitude approach to characterize diffusion[37].

Nevertheless, an additional explanation for this behavior can be extracted from the defect chemistry of SrTiO$_3$. For a diffusion of Sr via A-site-vacancies the general relationship between the diffusion coefficients for Sr D^{Sr} and Sr-vacancies $D^{V_{Sr}''}$ is

$$D^{Sr} = \frac{[V_{Sr}'']}{[Sr_{Sr}^x]} \cdot D^{V_{Sr}''} \tag{3}$$

where $[V_{Sr}'']/[Sr_{Sr}^x]$ is the vacancy concentration. While Ti is the slowest species, its diffusion is coupled to the strontium vacancies[15, 16], whereas equation (3) can be used as estimation for the diffusion constant relevant for sintering.

Taking into account the simplified defect chemistry for the bulk material SrTiO₃, the following cases have to be distinguished:

i. For undoped SrTiO3 in air the thermally activated vacancy concentration is:

$$[V_{Sr}''] \approx C_V \cdot e^{\left(-\frac{E_V}{k_B \cdot T}\right)} \quad for\ constant\ p_{O_2} \tag{4}$$

ii. For undoped SrTiO₃ in reducing atmosphere $[V_{Sr}'']$ decreases with decreasing oxygen partial pressure:

$$[V_{Sr}'']^{\frac{1}{6}} \approx p_{O_2} \quad for\ constant\ T \tag{5}$$

iii. For acceptor-doped SrTiO3 $[V_{Sr}'']$ decreases with increasing dopant concentration:

$$[V_{Sr}''] \sim \frac{1}{[A']} \quad for\ constant\ T\ and\ p_{O_2} \tag{6}$$

According equation to (5) and the high temperature (1450°C) defect chemistry of SrTiO₃[6], decreasing the oxygen partial pressure from 1 bar to $1 \cdot 10^{-15}$ bar results in a decrease of the diffusion coefficient of around two orders of magnitude. Following equation (6) increasing the acceptor dopant concentration has the same effect, but much stronger. Even with the existing variance this trend can be clarified by the decrease in the mean diffusions coefficient from $8 \cdot 10^{-18}\ m^2/s$ for the undoped SrTiO₃ down to $8 \cdot 10^{-21}\ m^2/s$ for 5% Fe-doped material.

The space charge theory provides a possible explanation for the change of the diffusion mechanism shown in Fig. 3 a). SrTiO₃ is well known for a positive charge in the Ti-rich grain boundary core[7, 17, 18] leading to an adjacent negative space charge region. Following a proposed model of Yan et al.[41] this leads to an area of enhanced diffusion. In undoped SrTiO₃ the space charge region has an extent around 100 nm[4]. Following the space charge theory, creating higher defect concentrations by increasing temperature, decreasing oxygen partial pressure or doping leads to a collapse of the range of the space charge. Therefor the area of enhanced diffusion decreases relative to the volume of the grains. At equal grain sizes this decrease could be leading to a switch from grain boundary diffusion to volume diffusion as it is present for the change from air to reducing atmosphere. The change of the diffusion mechanism may overlie the pure defect chemical effect described above. For the 2% doped SrTiO₃ the inhibit grain growth leads to comparable specific areas of enhanced diffusion as in the undoped system. Therefor both materials exhibit grain boundary diffusion as dominant mechanism for the densification. For the 5% material the Coble model is not applicable to achieve information about the diffusion path.

3.4 Impact of microstructural Morphology on Densification

fast shrinkage which would be expected just by looking at the grain size as driving force. In contrast, the material with 2% Fe-dopant can overcome this problem by incipient grain growth. Therefor the initial shrinkage of the iron doped material up to 70-75% relative density is rapid (Fig. 2). Afterwards

the 2% material is dependent on the grain growth while the 5% material shows a sharp kink in the densification rate.

The driving force for densification and grain growth is the surface energy and the free surface of the material. We assume the surface energy as constant and independent of the defect chemical changes in this experimental setup as for $SrTiO_3$ and Al_2O_3 only small variations of the surface energy are reported[34, 44, 45]. This point is still under discussion as there might be a change of the surface energy for example by segregation of dopants to the grain boundary, but there is no evidence for this argument found.

The free surface in the powder compact can be reduced by densification and grain growth with the curvature as driving force. Normally these both processes are seen contrary to each other. Taking the surface energy as constant driving force, the changes in the microstructural evolution (Fig. 4) can be explained by the different interaction between grain growth and densification. The densification rates plotted against the grain size and the density (Fig. 3) reveals the influence of the particular mechanism.

In the undoped material the microstructural evolution is nearly independent of the atmosphere. The densification rates show similar behavior with increasing grain size and increasing density. Both grain growth and densification occur simultaneously (Fig. 5) and in reducing atmosphere grain growth is slightly emphasized. The lower densification in reducing atmosphere can be explained with the switch in the diffusion mechanism and the decrease of the driving force due to the increased grain growth. In contrast to that with increasing doping level densification is more and more favorable compared to grain growth to reduce the free surface. For the 2% iron doped material the grain growth is bimodal and suppressed while for the 5% iron doped $SrTiO_3$ the inner energy is reduced only by densification while no grain growth is present. With decreasing grain growth one would expect higher driving forces for densification. Lower densification rates with increasing dopant level support the proposed decrease in the diffusion coefficient. An interesting fact is that at equal grain sizes the densification rates get lower with increasing iron doping (Fig. 3 a) but compared to the undoped material the final densities are higher for $SrTiO_3$ with 2% iron and much lower for $SrTiO_3$ with 5% iron (Fig. 2).

The microstructural evolution offers a potential explanation for that behavior. Pore shrinkage or pore growth depending on the size and coordination number of the pore as shown in Fig. 7 is a well know phenomena[46, 47, 48] which is nicely applicable for $SrTiO_3$. For a constant dihedral angle at the triple junction of 120°, which is equal to six surrounding grains the pore would be stabilized. Coordination numbers smaller six means pore shrinkage (Fig. 7 a) while pores with large numbers of grains attached tend to grow (Fig. 7 b).
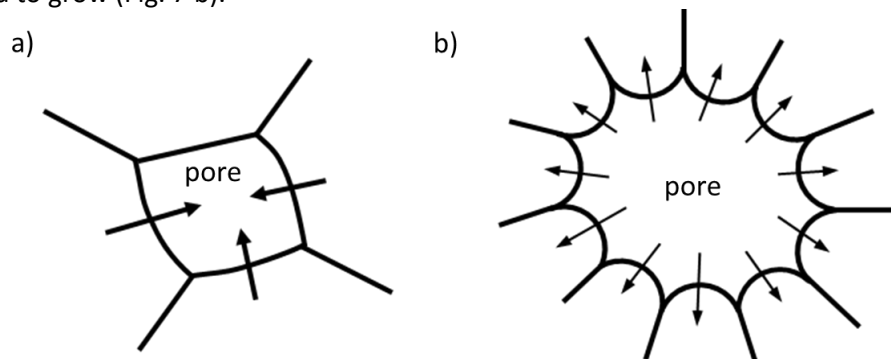

Fig. 7: Scheme of a shrinking pore with

In the undoped $SrTiO_3$ the coordination number of the pores is always ≤ 6, reduced by the present grain growth during the sintering process (Fig. 8 a).

For the 2% iron doped material we believe the concept of grain growth induced densification[49, 50] is responsible for the achievable high end densities. Due to the bimodal grain growth starting around 80-85% relative density, larger pores can change their coordination number and therefore be activated to contribute to the overall densification.

For the highly doped material we can see a cluster wise densification in the early stage of sintering, leaving behind large pores in relation to the grain size (Fig. 4 g). Further densification can only take place at small pores with several grains attached reducing the overall densification rates drastically. At large pores the curvature provides no longer a driving force for shrinkage. The shrinkage at fine pores, with little grains attached (Fig. 7 a), is very fast during the heating, while slightly larger, disadvantageous coordinated pores tend to grow (Fig. 7 b). The sharp drop in the densification rates by a slight increase in density clearly supports this argument (Fig. 3 b).

This might be caused by the initial state of a green body where the pores show a size distribution. As no grain growth is apparent the coordination number at the large pores is not able to decrease during the holding time and further densification is impossible. The result is a microstructure consisting of clusters with 100% local density and large pores normally surrounded by more than 10 grains (Fig. 8 b) leading to an overall density of maximum 80%.

These results clearly show that grain growth is not always contrary to densification but can be utilized to achieve high end densities even in materials with nominal lower densification rates.
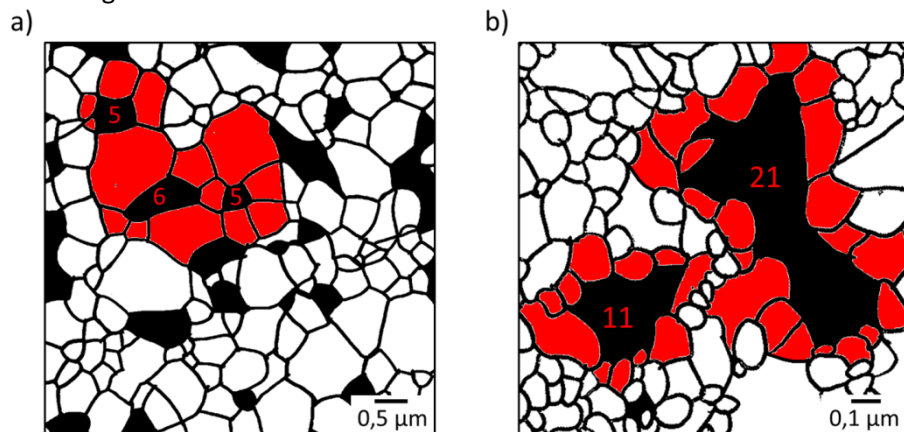
**Fig. 8: Coordination number of undoped and 5%-SrTiO₃**

3.5 Grain Growth and Sintering

#vom verdichtungsteil hiehergeschoben

The grain growth behavior during isothermal sintering is shown in **Fehler! Verweisquelle konnte nicht gefunden werden.** along with fits of a standard grain growth law

$$G^2 - G_0^2 = k \cdot t \qquad (7)$$

with the mean grain diameter G, the mean diameter G_0 at time $t = 0$ and the grain growth constant k ###cite burke and turnbull 1952###. In **Fehler! Verweisquelle konnte nicht gefunden werden.**, the mean grain size is plotted for different holding times. For undoped material, D_0 is higher by a factor of 2 compared to doped material. The undoped material starts with factor two larger grains and has slightly higher growth rates in reducing atmosphere. With increasing dopants the grain growth is strongly inhibited and disappears at 5% iron doping completely in this temperature regime.
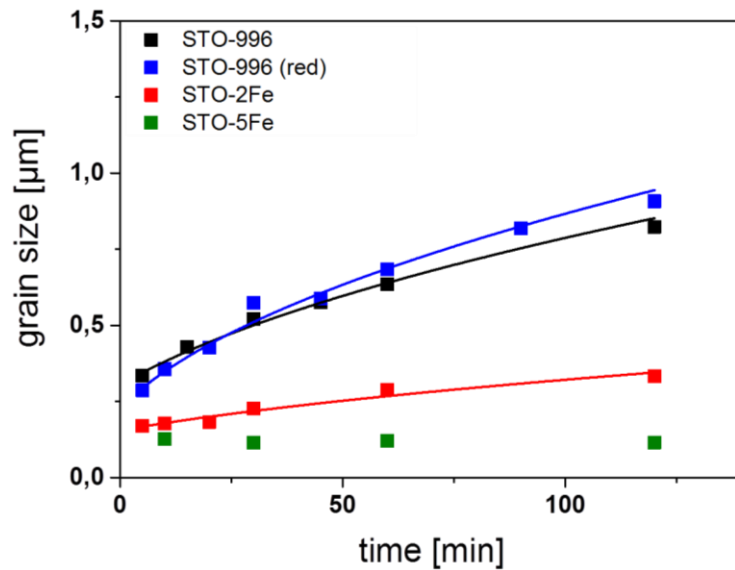
Fig. 9: Grain growth during isothermal sintering

Not only the densification has to be considered to evaluate the microstructural evolution, but also the grain growth plays an important role. The grain growth behavior plotted in **Fehler! Verweisquelle konnte nicht gefunden werden.** shows slightly higher grain growth in reducing atmosphere and a drastic decrease with increasing doping level compared to undoped SrTiO₃ in air.

Fitting the cubic law **Fehler! Verweisquelle konnte nicht gefunden werden.** to the experimental data in **Fehler! Verweisquelle konnte nicht gefunden werden.** gives us values for the grain growth constant K which are drawn into the Arrhenius graph of Fig. 10. The other data points represent grain growth measurements on undoped SrTiO₃ in air. While the samples of Rheinheimer et al. [33] were pre sintered to exclude densification effects the samples of Bäurer et al.[29] were sintered during the heat treatment for the grain growth experiment. Nevertheless the grain growth constants K are in good agreement with each other. This means that grain growth in dense SrTiO₃, during the sintering process and directly adjacent to sintering shows no differences. Inhibiting effect on grain growth due to pore drag effects could not be observed and do not affect the microstructural evolution.
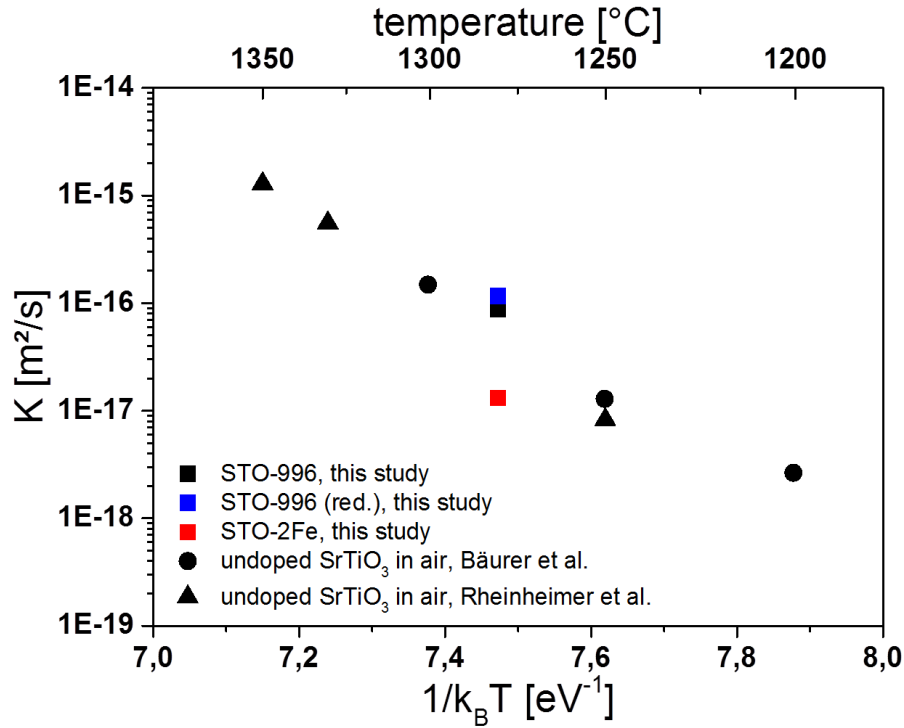
Fig. 10: grain growth coefficients in compare

For samples sintered in reducing atmosphere the grain growth is slightly faster than in air. This effect is still under investigation and not yet fully understood. One possible explanation is the change of the surface and grain boundary energy with decreasing oxygen partial pressure identified by Rheinheimer et al.[34]. Chung et al.[39, 40] provide another approach depending on the total defect concentration in the material. They discovered a change in the grain boundary mobility due to a switch from rough to a facetted grain boundaries with increasing defect concentration in $SrTiO_3$, accelerating the grain growth. Regarding this idea, the space charge concept mentioned above might also play a role for grain growth by changing the concentration profile adjacent to the boundary.

For the iron doped $SrTiO_3$ grain growth experiments are hard to conduct, considering the bimodal grain growth in $SrTiO_3$ with 2% iron (Fig. 4 e, f) and the low density combined with inhibit grain growth for the 5% iron doped $SrTiO_3$ (Fig. 4 g, h). Further information about a change of the surface energy or the mobility of the grain boundary dependent on doping in $SrTiO_3$ is unknown. Solute segregation of defects, especially an enrichment of the grain boundary with acceptor atoms, is reported for $SrTiO_3$[17, 18, 51]. Therefor an explanation could be given by applying the idea of solute drag[52, 53]. The segregation profile adjacent to the grain boundary can be seen as a force contrary to the grain boundary movement[52]. Alternative the mobility of the boundary is limited by the movement of the segregation profile. While the width of the segregation is not very large, we could show the limited diffusion with increasing iron doping, possibly leading to the slower movement of the segregation profile. For 2% iron doping some of the boundaries might be energetically able to drag from the segregation profile leading to increased grain growth and a bimodal microstructure. For the 5% iron doped $SrTiO_3$ the barrier created by the strong segregation seems to be much higher leading to evanescent grain growth in the observed time regime.

4   Summary and Conclusions

Acknowledgement

References

1. R. A. De Souza, J. Fleig, R. Merkle, and J. Maier, "SrTi0(3): a model electroceramic," *Z Metallkd,* 94[3] 218-25 (2003).
2. A. S. Bhalla, R. Guo, and R. Roy, "The perovskite structure – a review of its role in ceramic science and technology," *Mat Res Innovat,* 4[1] 3-26 (2000).
3. R. Waser, "Bulk Conductivity and Defect Chemistry of Acceptor-Doped Strontium-Titanate in the Quenched State," *Journal of the American Ceramic Society,* 74[8] 1934-40 (1991).
4. M. Vollman and R. Waser, "Grain-Boundary Defect Chemistry of Acceptor-Doped Titanates - Space-Charge Layer Width," *Journal of the American Ceramic Society,* 77[1] 235-43 (1994).
5. R. Hagenbeck, L. SchneiderStormann, M. Vollmann, and R. Waser, "Numerical simulation of the defect chemistry and electrostatics at grain boundaries in titanate ceramics," *Mat Sci Eng B-Solid,* 39[3] 179-87 (1996).
6. R. Moos and K. H. Hardtl, "Defect chemistry of donor-doped and undoped strontium titanate ceramics between 1000 degrees and 1400 degrees C," *Journal of the American Ceramic Society,* 80[10] 2549-62 (1997).
7. R. Waser, "Electronic-Properties of Grain-Boundaries in Srtio3 and Batio3 Ceramics," *Solid State Ionics,* 75 89-99 (1995).
8. R. Hagenbeck and R. Waser, "Simulation of electrical properties of grain boundaries in titanate ceramics," *Ber Bunsen Phys Chem,* 101[9] 1238-41 (1997).
9. R. Moos and K. H. Hardtl, "Dependence of the Intrinsic Conductivity Minimum of Srtio3 Ceramics on the Sintering Atmosphere," *Journal of the American Ceramic Society,* 78[9] 2569-71 (1995).
10. R. A. De Souza, V. Metlenko, D. Park, and T. E. Weirich, "Behavior of oxygen vacancies in single-crystal SrTiO3: Equilibrium distribution and diffusion kinetics," *Phys Rev B,* 85[17] (2012).
11. P. Lupetin, "Charge carrier defect chemistry of nanoscopic SrTiO 3," pp. XX, 139 S. in., 2012.
12. W. H. Rhodes and W. D. Kingery, "Cation Dislocation Pipe Self-Diffusion in Srtio3," *Am Ceram Soc Bull,* 44[8] 635-& (1965).
13. W. H. Rhodes and W. D. Kingery, "Dislocation Dependence of Cationic Diffusion in Srtio," *Journal of the American Ceramic Society,* 49[10] 521-& (1966).
14. M. J. Akhtar, Z. U. N. Akhtar, R. A. Jackson, and C. R. A. Catlow, "Computer-Simulation Studies of Strontium-Titanate," *Journal of the American Ceramic Society,* 78[2] 421-28 (1995).
15. K. Gomann, G. Borchardt, A. Gunhold, W. Maus-Friedrichs, and H. Baumann, "Ti diffusion in La-doped SrTiO3 single crystals," *Phys Chem Chem Phys,* 6[13] 3639-44 (2004).
16. K. Gomann, G. Bochardt, M. Schulz, A. Gomann, W. Maus-Friedrichs, B. Lesage, O. Kaitasov, S. Hoffman-Eifert, and T. Schneller, "Sr diffusion in undoped and La-doped SrTiO3 single crystals under oxidizing conditions," *Phys Chem Chem Phys,* 7[9] 2053-60 (2005).
17. Y. M. Chiang and T. Takagi, "Grain-Boundary Chemistry of Barium-Titanate and Strontium-Titanate .1. High-Temperature Equilibrium Space-Charge," *Journal of the American Ceramic Society,* 73[11] 3278-85 (1990).
18. Y. M. Chiang and T. Takagi, "Grain-Boundary Chemistry of Barium-Titanate and Strontium-Titanate .2. Origin of Electrical Barriers in Positive-Temperature-Coefficient Thermistors," *Journal of the American Ceramic Society,* 73[11] 3286-91 (1990).
19. I. Denk, J. Claus, and J. Maier, "Electrochemical investigations of SrTiO3 boundaries," *J Electrochem Soc,* 144[10] 3526-36 (1997).
20. R. Hagenbeck and R. Waser, "Detailed temperature dependence of the space charge layer width at grain boundaries in acceptor-doped SrTiO3-ceramics," *J Eur Ceram Soc,* 19[6-7] 683-86 (1999).
21. R. Hagenbeck, "Electrical properties of grain boundaries in titanate ceramics," *Sol St Phen,* 80-81 21-32 (2001).
22. R. A. De Souza and M. Martin, "Using O-18/O-16 exchange to probe an equilibrium space-charge layer at the surface of a crystalline oxide: method and application," *Phys Chem Chem Phys,* 10[17] 2356-67 (2008).

23. R. A. De Souza, "The formation of equilibrium space-charge zones at grain boundaries in the perovskite oxide SrTiO3," *Phys Chem Chem Phys,* 11[43] 9939 (2009).

24. S. von Alfthan, N. A. Benedek, L. Chen, A. Chua, D. Cockayne, K. J. Dudeck, C. Elsässer, M. W. Finnis, C. T. Koch, B. Rahmati, M. Rühle, S.-J. Shih, and A. P. Sutton, "The Structure of Grain Boundaries in Strontium Titanate: Theory, Simulation, and Electron Microscopy," *Annual Review of Materials Research,* 40[1] 557-99 (2010).

25. M. Vollmann, "Elektronische Korngrenzeigenschaften akzeptordotierter SrTiO 3 -Dielektrika," pp. IX, 132 S. in Fortschrittberichte VDI : Reihe 9, Elektronik, Mikro- und Nanotechnik ; 246. VDI-Verl., Düsseldorf, 1997.

26. F. Poignant and J. Juda, "The Formation of Grain Boundary Potential Barriers in Semiconducting (Sr,Ca)(Ti,Nb)O$_3$ Ceramics," *Key Engineering Materials,* 132-136 1337-40 (1997).

27. R. Meyer, R. Waser, J. Helmbold, and G. Borchardt, "Observation of vacancy defect migration in the cation sublattice of complex oxides by O-18 tracer experiments," *Phys Rev Lett,* 90[10] (2003).

28. M. Baurer, H. Kungl, and M. J. Hoffmann, "Influence of Sr/Ti Stoichiometry on the Densification Behavior of Strontium Titanate," *Journal of the American Ceramic Society,* 92[3] 601-06 (2009).

29. M. Baurer, D. Weygand, P. Gumbsch, and M. J. Hoffmann, "Grain growth anomaly in strontium titanate," *Scripta Mater,* 61[6] 584-87 (2009).

30. M. Baurer, H. Stormer, D. Gerthsen, and M. J. Hoffmann, "Linking Grain Boundaries and Grain Growth in Ceramics," *Adv Eng Mater,* 12[12] 1230-34 (2010).

31. M. Baurer, S. J. Shih, C. Bishop, M. P. Harmer, D. Cockayne, and M. J. Hoffmann, "Abnormal grain growth in undoped strontium and barium titanate," *Acta Mater,* 58[1] 290-300 (2010).

32. L. Amaral, A. M. R. Senos, and P. M. Vilarinho, "Sintering kinetic studies in nonstoichiometric strontium titanate ceramics," *Mater Res Bull,* 44[2] 263-70 (2009).

33. W. Rheinheimer and M. J. Hoffmann, "Non-Arrhenius behavior of grain growth in strontium titanate: New evidence for a structural transition of grain boundaries," *Scripta Mater,* 101[0] 68-71 (2015).

34. W. Rheinheimer, M. Baurer, H. Chien, G. S. Rohrer, C. A. Handwerker, J. E. Blendell, and M. J. Hoffmann, "The equilibrium crystal shape of strontium titanate and its relationship to the grain boundary plane distribution," *Acta Mater,* 82 32-40 (2015).

35. W. Rheinheimer, M. Bäurer, C. A. Handwerker, J. E. Blendell, and M. J. Hoffmann, "Growth of single crystalline seeds into polycrystalline strontium titanate: Anisotropy of the mobility, intrinsic drag effects and kinetic shape of grain boundaries," *Acta Mater,* 95[0] 111-23 (2015).

36. R. L. Coble, "Intermediate-Stage Sintering - Modification and Correction of a Lattice-Diffusion Model," *J Appl Phys,* 36[7] 2327-& (1965).

37. R. L. Coble, "Sintering Crystalline Solids .1. Intermediate and Final State Diffusion Models," *J Appl Phys,* 32[5] 787-& (1961).

38. R. L. Coble, "Sintering Crystalline Solids .2. Experimental Test of Duffusion Models in Powder Compacts," *J Appl Phys,* 32[5] 793-& (1961).

39. S. Y. Chung, S. J. L. Kang, and V. P. Dravid, "Effect of sintering atmosphere on grain boundary segregation and grain growth in niobium-doped SrTiO3," *Journal of the American Ceramic Society,* 85[11] 2805-10 (2002).

40. S. Y. Chung, D. Y. Yoon, and S. J. L. Kang, "Effects of donor concentration and oxygen partial pressure on interface morphology and grain growth behavior in SrTiO3," *Acta Mater,* 50[13] 3361-71 (2002).

41. M. F. Yan, R. M. Cannon, H. K. Bowen, and R. L. Coble, "Space-Charge Contribution to Grain-Boundary Diffusion," *Journal of the American Ceramic Society,* 60[3-4] 120-27 (1977).

42. T. K. Gupta and R. L. Coble, "Sintering of Zno .1. Densification and Grain Growth," *Journal of the American Ceramic Society,* 51[9] 521-& (1968).

43. T. K. Gupta, "Sintering of Mgo - Densification and Grain Growth," *J Mater Sci,* 6[1] 25-& (1971).

44. C. A. Handwerker, J. M. Dynys, R. M. Cannon, and R. L. Coble, "Dihedral Angles in Magnesia and Alumina - Distributions from Surface Thermal Grooves," *Journal of the American Ceramic Society,* 73[5] 1371-77 (1990).

45. M. X. Jin, E. Shimada, and Y. Ikuma, "Grain boundary grooving by surface diffusion in SrTiO3 bicrystal," *J Mater Res,* 14[6] 2548-53 (1999).

46. W. D. Kingery, H. K. Bowen, and D. R. Uhlmann, "Introduction to ceramics," pp. XII, 1032 S. 2. ed. ed. Wiley: New York [u.a.], (1976).

47. S.-J. L. Kang, "Sintering : densification, grain growth, and microstructure," pp. XII, 265 S. Elsevier Butterworth-Heinemann: Amsterdam, (2005).

48. M. N. Rahaman, "Sintering of ceramics," pp. 388 S. CRC Press: Boca Raton, Fla. [u.a.], (2008).

49. F. F. Lange and B. J. Kellett, "Thermodynamics of Densification .2. Grain-Growth in Porous Compacts and Relation to Densification," *Journal of the American Ceramic Society,* 72[5] 735-41 (1989).

50. B. J. Kellett and F. F. Lange, "Thermodynamics of Densification .1. Sintering of Simple Particle Arrays, Equilibrium-Configurations, Pore Stability, and Shrinkage," *Journal of the American Ceramic Society,* 72[5] 725-34 (1989).

51. N. Wilcox, V. Ravikumar, R. P. Rodrigues, V. P. Dravid, M. Vollmann, R. Waser, K. K. Soni, and A. G. Adriaens, "Investigation of Grain-Boundary Segregation in Acceptor and Donor-Doped Strontium-Titanate," *Solid State Ionics,* 75 127-36 (1995).

52. J. W. Cahn, "The impurity-drag effect in grain boundary motion," *Acta Metall Mater,* 10[9] 789-98 (1962).

53. S. G. Kim and Y. B. Park, "Grain boundary segregation, solute drag and abnormal grain growth," *Acta Mater,* 56[15] 3739-53 (2008).